Article

Flexible Operation of Concentrating Solar Power Plant with Thermal Energy Storage Based on a Coordinated Control Strategy

Xianhua Gao [1], Shangshang Wei [2], Chunlin Xia [1] and Yiguo Li [1],*

[1] National Engineering Research Center of Power Generation Control and Safety, School of Energy and Environment, Southeast University, Nanjing 210096, China; 230189044@seu.edu.cn (X.G.); 230208067@seu.edu.cn (C.X.)

[2] College of Energy and Electrical Engineering, Hohai University, Nanjing 211100, China; weishsh@hhu.edu.cn

[*] Correspondence: lyg@seu.edu.cn; Tel.: +86-139-1397-0596

Abstract: With the ambition of achieving carbon neutrality worldwide, renewable energy is flourishing. However, due to the inherent uncertainties and intermittence, operation flexibility of controllable systems is critical to accommodate renewables. Existing studies mainly focus on improving the flexibility of conventional plants, while no attention has been paid to the flexible operation of concentrating solar power with thermal energy storage (CSP-TES) systems. To this end, the ultimate goal of this work is to investigate the potentiality and realization of CSP-TES systems to flexibly operate in grid system regulation. With this goal, the dynamic characteristics of a 50 MW parabolic trough collector CSP plant with molten-salt-based TES is analyzed, and its dominant control characteristics are concluded to demonstrate the possibility of the ideal. After that, a coordinated control strategy is proposed. Specifically, a disturbance observer-based feedforward–feedback control scheme and a feedforward–feedback controller are designed, respectively, for the solar field and the energy storage subsystems, while the power block subsystem is regulated by a two-input and two-output decoupled controller. Based on the decentralized structure, three simulation cases are, respectively, performed to testify the capacity of the CSP-TES system to wide-range load variation tracking, strong disturbance rejection, or both. The results show that the CSP-TES system can adequately track the grid commands based on the proposed coordinated control strategy, even under strong fluctuation of irradiation, demonstrating the flexibility of CSP-TES participating in grid regulation. In the context of continuous penetration of renewable energy into the grid system, research on the role transition of the CSP-TES system from its own optimization to grid regulator is of great importance.

Keywords: concentrating solar power plants; flexible operation; control strategy; disturbance rejection

1. Introduction

With worldwide commitment to the ambitious goal of carbon neutrality, the penetration of renewable energy will inevitably increase [1,2]. However, the electrical grid system, under high penetration of renewable energy, will face many unavoidable challenges due to the strong uncertainty of renewable sources, such as security, stability and reliability [3,4]. In order to alleviate the impact of uncertainties on the grid system, exploiting controllable power generation plants to maintain the quality requirements of grid system is a necessity. Among them, flexible operation of conventional fossil fuel plants has gained unprecedented increasing attention. However, affordable accommodation for renewable energy of a conventional coal power plant is usually limited at 50% of the rated capacity because of various physical constraints in energy conversion processes [5]. In addition, the fossil fuel plants produce a large amount of carbon dioxide, causing their decommission in some countries [6]. There are many alternative power generation plants. Solar power plants, as a commercially mature technology, is one such alternative, and has even taken a large market share in the grid system. For this reason, this paper attempts to investigate the possibility

of solar power plants, specifically the concentrating solar power plant with thermal energy storage (CSP-TES) system, to operate flexibly in the regulation of the electrical grid system.

The CSP-TES system has an interesting characteristic of dispatchability, essentially due to the coordination function of the thermal energy storage subsystem. This characteristic has been mentioned by several works. For instance, ref. [7] examined the dispatchability by using two country cases of Morocco and Algeria, and found that cost advantages of CSP with TES should be highlighted when the gird system is in high renewable penetration. Ref. [8] also concluded that CSP with TES can provide dispatchable energy and power based on the operation date of Andasol 3, and such an advantage enables the CSP to have many attractive functions. Based on the review of CSP plant development and operation market rules in eight countries, ref. [9] concluded that CSP's dispatchability and flexibility should be highly valued and encouraged by markets and policies. The influences of dispatchability on the CSP system are also investigated in many works [10–12].

However, the dispatchability of CSP-TES is mostly applied to economic dispatch in existing works, where the basic idea is to firstly establish model constraints according to equipment characteristics, and then optimize a specific objective function and calculate the schedule of the CSP-TES via various operation strategies. For instance, a mixed-integer linear problem was also established by Kost et al. to maximize both the operational profit and investment annuity of a CSP plant over the planning horizon [13]. Similarly, a mixed-integer programming model of a CSP-TES plant was proposed in ref. [10]. In addition, a model predictive control operation strategy was also exploited to minimize the objective composed of tracking the schedule and generating the optimal schedule for the next day. Studies of optimal operation strategy of CSP-TES can also be found in many works [14–16].

In fact, the optimal schedules of CSP-TES have to be delivered to controllers of subsystems. In existing works, the controllers are designed mainly from a subsystem level in a decoupling way, as the coupling effects among subsystems are considered in the scheduling layer. Extensive works based on the decoupling way have been reported. For instance, a nonlinear model-based adaptive control strategy has been proposed to control the outlet temperature of a parabolic trough plant [17]. An optimal model predictive control with lump disturbance to maintain the outlet temperature has been proposed [18]. A linear quadratic regulator was designed to regulate the output oil enthalpy of the thermal storage subsystem in ref. [19]. This idea of controller design can be found in many studies [20,21].

However, whether optimal dispatch or controller design of the studies as previously mentioned, they are all carried out without considering CSP participation in the regulation of the grid system. Therein, CSP can calculate the best performance itself through optimal operation strategies, and then approach this self-optimization by tracking the optimized instructions, without considering the contribution to the performance of the grid system.

In contrast, the work here studies the flexible operation of CSP-TES and investigates its potential function in grid regulation, based on its dispatchable capability. Different from the traditional approach, when the CSP-TES participates in the grid regulation, the power instruction is not obtained from its own optimization, but delivered from the grid operator. This indicates that the role of the CSP-TES transfers from independent optimal operation to a clean regulator of the grid system. Regarding the capability of the role transition of CSP-TES, it has been claimed by [8] that CSP can offer similar operational attributes as conventional power plants, and can also support regulation and frequency response. However, the similarities and differences between CSP and conventional plants, and how to realize the flexible regulation of CSP-TES, have not yet been studied. To this end, dynamic characteristics of the CSP-TES system is investigated based on the dynamic model in ref. [22], and a coordinated control strategy is further proposed to realize the flexible operation of CSP-TES. To the authors' best knowledge, research on CSP-TES from this perspective has not yet been conducted.

This work is a further extension of our previous work [22], and organized as follows. Section 2 examines the dynamic characteristics of CSP-TES in ref. [22], and analyzes its control-oriented characteristics for flexible operation. Afterwards, a coordinated control

strategy is designed in Section 3. Section 4 testifies the capacity of CSP-TES to operate flexibly in grid regulation by case studies even under wide-range operation and subjected to strong uncertain irradiation. Finally, conclusions are drawn in Section 5.

2. Dynamic Simulation and Control Characteristic Analysis

An in-depth understanding of the controlled system is critical to controller design. Figure 1 shows the schematic diagram of a parabolic trough CSP with TES, where it consists of solar field (SF), TES and power block (PB) subsystems. In control practice, the SF outlet temperature of heat transfer fluid (HTF) and its efficiency are dominated by the HTF flowrate of SF; electricity generation and main steam pressure of PB are controlled by HTF flowrate and the opening valve of the PB subsystem; the thermal charging/discharging of TES is manipulated by the MS flowrate of TES; and solar irradiation is the energy input of the CSP system. Consequently, typical step change in process control engineering is performed to evaluate the control characteristics of the CSP-TES system. In this work, the CSP-TES is assumed on a sunny day where the TES subsystem is under charging state.

Figure 1. Schematic diagram and energy flows of a parabolic trough concentrating solar power (CSP) plant [22].

For this system, we have established a system-level analytical model in the form of the ordinary differential equations in ref. [22], whose accuracy has been verified by the steady-state and dynamic tests. Therefore, it can be reliably applied to design controllers of CSP plants. Then, based on the analytical model and with the given stable operating parameters in Table 1, the system step response is analyzed as follows.

Table 1. Operating parameters under steady-state operation condition.

Parameters	Value	Parameters	Value
Irradiation	700 W/m^2	Heat transfer fluid (HTF) flowrate to thermal energy storage (TES)	700 kg/s
Solar field (SF) HTF flowrate	90 kg/s	HTF flowrate to power block (PB)	500 kg/s
SF HTF outlet temperature	390.6 °C	Power generation	41.8 MW
Hot molten salt (MS) temperature	380.8 °C	Opening of main valve	0.9
Cold MS temperature	25 °C	Pressure of turbine inlet	9.43 MPa

2.1. System Response to Step Change of HTF Flowrate of SF

Figure 2 shows the system response to step change of HTF flowrate of SF. As can be seen, the HTF flowrate of SF has a strong effect on the controlled variables of the system. When the HTF flowrate increases, the SF outlet temperature decreases gradually as the input solar energy remains. The decrease of SF outlet temperature further leads to the reduction in electricity and main steam pressure. Because the HTF flowrate to PB remains at 500 kg/s, the lower HTF temperature to PB weakens the heat transfer of heat exchangers, which causes less energy to be transferred to steam. Conversely, the MS temperature increases first as the HTF flowrate of SF steps. This increase is attributed to more HTF flowrate delivered to the TES subsystem. However, as the SF outlet HTF temperature further decreases, the heat transfer efficiency of the HTF-MS heat exchanger degrades, which leads to the decline of MS temperature. However, the responses are not monotonous, as all the chosen variables climb again after about 900 s. Such behaviors maybe be due to the increase in inlet HTF temperature of SF, and this increase contributes to the increases in SF outlet HTF temperature. With the SF outlet HTF temperature increasing, the MS outlet temperature, the electricity and the main steam pressure climb smoothly to new steady states.
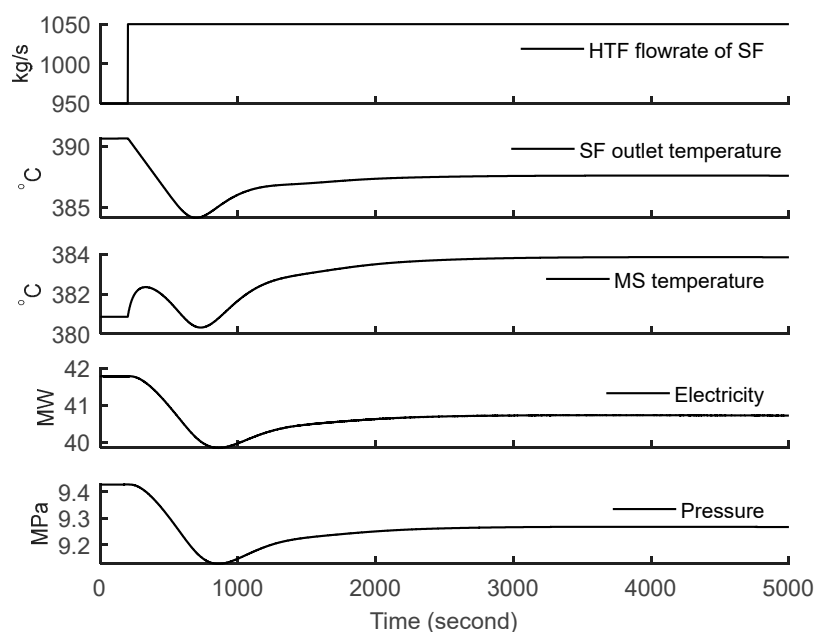
Figure 2. System response to step change of HTF flowrate of SF.

2.2. System Response to Step Change of HTF Flowrate of PB

As the inlet HTF flowrate of PB increases, more steam is generated because the heat transfer capacity in the heat exchanger train is enhanced, thereby resulting in a monotonous increase in the electricity, together with the steam pressure. These indicate that the response characteristics of CSP with TES are similar to conventional plants. Meanwhile, the change

of inlet HTF flowrate of PB also affects the SF outlet HTF temperature and MS temperature, as proven in Figure 3. However, the MS outlet temperature responds quickly, while the HTF temperature changes later, with a time delay of about 500 s. This is because the decrease of the HTF flowrate of TES subsystem leads to the increase of the HTF flowrate of PB, under the constant total HTF flowrate. Such a decrease leads to the drop in the MS outlet temperature in the TES. For SF outlet HTF temperature, although the total HTF flowrate in the SF is the same, the flowrate redistribution changes the SF inlet HTF temperature, and ultimately affects the SF outlet HTF temperature after a transport delay.
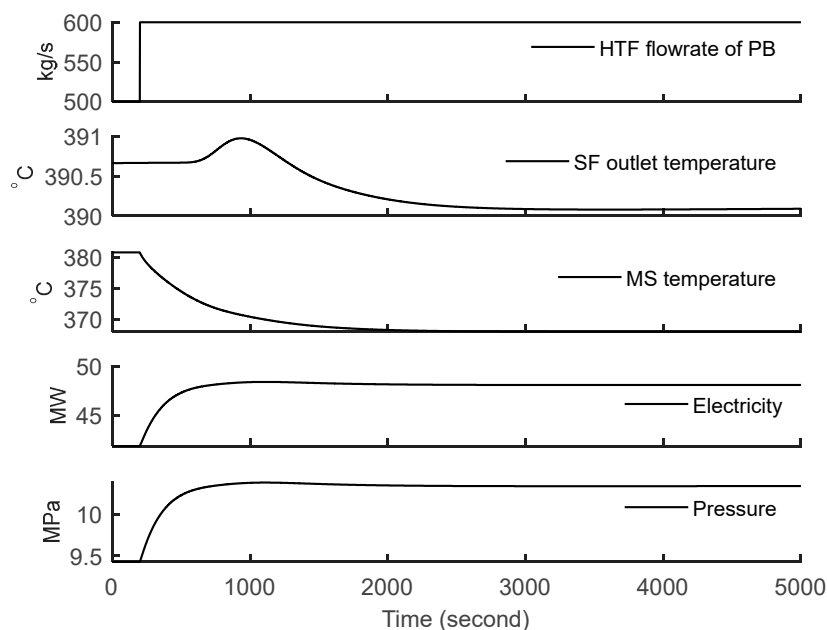
Figure 3. System response to step change of HTF flowrate of PB.

2.3. System Response to Step Change of Main Valve Opening

Figure 4 illustrates the system response to main valve opening steps. As can be seen, an increase in the opening of the main valve will instantly lead to an increase in electricity and a decrease in steam pressure, which is similar to conventional plants. However, the influence on MS temperature and SF outlet HTF temperature are not revealed because the changes of the main valve have a minor direct influence on the SF inlet HTF temperature, and indirect impact on the outlet temperature of SF and MS; nevertheless, the influence is very limited.

2.4. System Response to Step Change of MS Flowrate of TES

The step change of MS flowrate of TES also has an impact on system dynamics, as illustrated in Figure 5. When the MS flowrate steps, the MS temperature will drop instantly; however, the SF outlet HTF temperature decreases after a certain time delay. The reason is similar to that of system step response to HTF flowrate of PB; the two cases both reduce SF inlet HTF temperature directly, and ultimately reduce the SF outlet HTF temperature after a certain transport delay. The changes in SF outlet HTF temperature further impact on the performance of the PB subsystem, despite the impact being limited.

2.5. System Response to Step Change of Solar Irradiation

Solar irradiation is the input energy to CSP and has the features of uncertainty and uncontrollability. To this end, dynamic response of the CSP system to irradiation is examined in Figure 6. It can be seen from Figure 6 that step change of irradiation has a significant impact on the overall CSP system. With about 7.1% increase of solar irradiation, the SF outlet temperature and MS temperature both increase by around 8 °C, and the electricity

and main steam pressure increase by 7.1% and 3.8%, respectively. Since solar energy is intermittent and fluctuates strongly, the dynamic responses indicate the importance of disturbance rejection control. Moreover, solar energy has a very broad influence on system performance, as its increase leads to an increase in the SF outlet HTF temperature, and as a result, the performance of the downstream subsystem changes greatly. The slow decrease also suggests the large inertia of the CSP system.
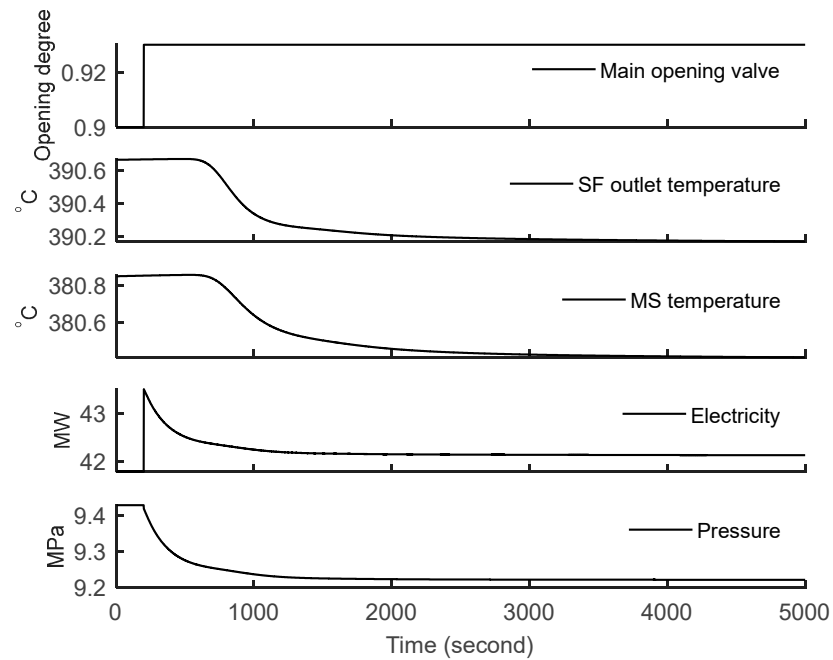
Figure 4. System response to step change of main valve opening.
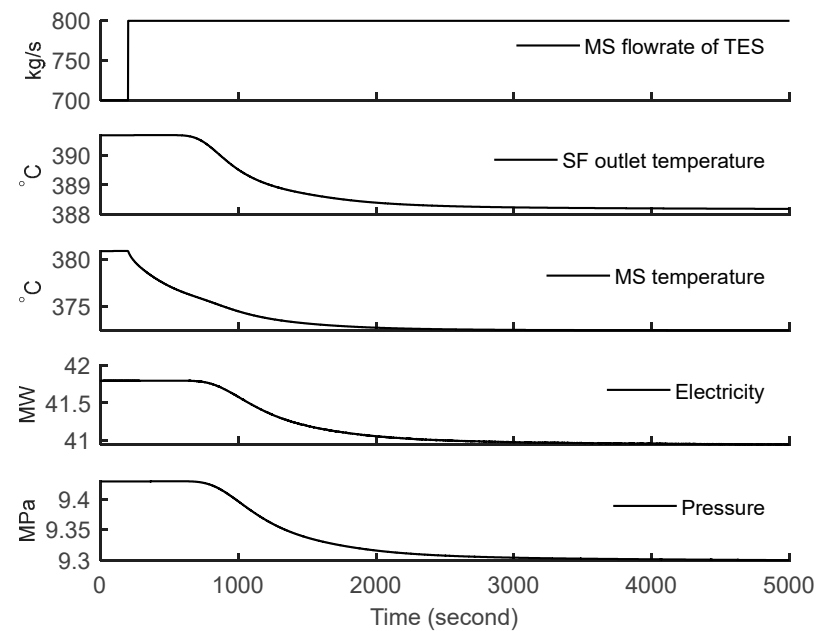
Figure 5. System response to step change of MS flowrate of TES.
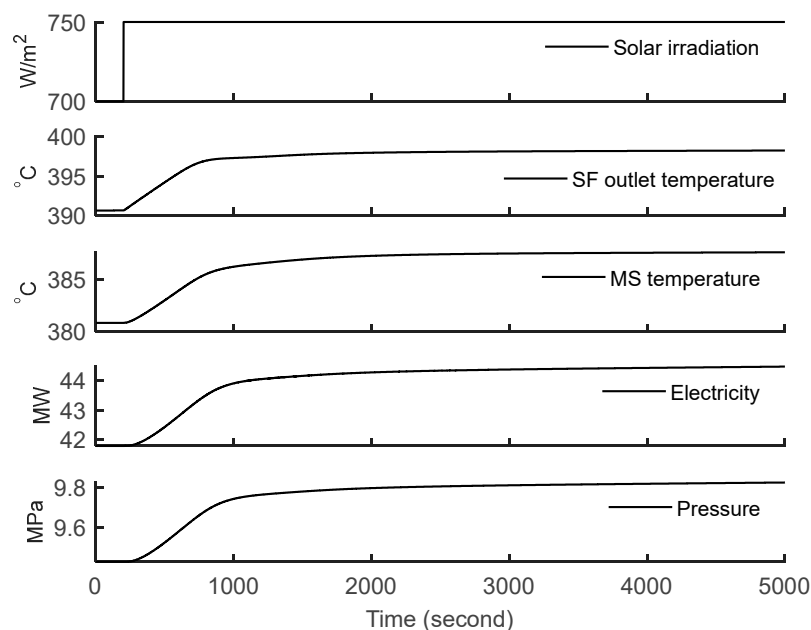
Figure 6. System response to step change of solar irradiation.

Based on the analysis above, it can be seen that there are many similarities between the dynamic characteristics of the CSP-TES and conventional fossil fuel plant. For instance, they are both a multivariable system with large thermal inertia and certain time delays. These similarities, to some degree, demonstrate the potential of CSP-TES to flexible operation. Nevertheless, there are also differences between CSP-TES and conventional plants.

(1) The CSP-TES system is a weak coupling system. Although the CSP-TES system comprises three subsystems, the dispatchability of the TES subsystem depresses the coupling degree between subsystems. The connection between SF and PB subsystems is dominantly the HTF temperature, as the HTF flowrate is determined automatically when HTF flowrate of SF and PB is controlled. Once the HTF temperature between SF and PB is controlled well, the SF and PB can be considered to be almost decoupled.

(2) The CSP-TES system is characterized by switch nonlinearity. The nonlinear behavior is determined by HTF flowrate of TES, which depends on the charging/discharging states of TES, while the states of TES are restricted by HTF flowrate between SF and PB. Under the assumption that TES is in charging state, the HTF flowrate of TES is equal to the HTF flowrate of SF minus the flowrate of PB, indicating that the flexible operation capacity of CSP system varies from that of conventional plants significantly.

(3) The CSP system is an uncertainty-dominated system. The largest uncertainty stems from the intermittence of solar energy, and the large variation in solar energy further deduces model mismatches and parameter variation, making the CSP system have strong uncertainties. Thus, from the perspective of disturbance rejection, it is necessary to attenuate the disturbance quickly from where it occurs to prevent solar energy fluctuations affecting the downstream subsystems. Consequently, disturbance rejection control of the CSP system should be a top priority.

3. Coordinated Control Strategy of CSP-TES System

According to the aforementioned control characteristics, and with the aim of flexible operation of the CSP-TES system, a coordinated control strategy was proposed, as shown in Figure 7. Since the CSP-TES system is a weak coupling system, decentralized proportional-integral-derivative (PID) controllers are designed, providing that the controllers can maximize the potential engineering application due to their simple structure and high maturity. As for uncertainty alleviation, a disturbance observer-based (DOB) feedforward–feedback scheme is designed and applied to the SF subsystem to reject the dis-

turbance of solar energy rapidly. For the PB subsystem, a decoupling controller is designed to decouple the electricity generation and main steam pressure, providing the similarities between the PB subsystem and traditional plants. The difference of HTF flowrate of SF and PB are fed forward to the TES, together with SF outlet HTF temperature, to compensate the switch nonlinearity. In addition, a feedback controller is designed to manipulate the MS flowrate of TES to control the MS temperature. Details of the control scheme are as follows.
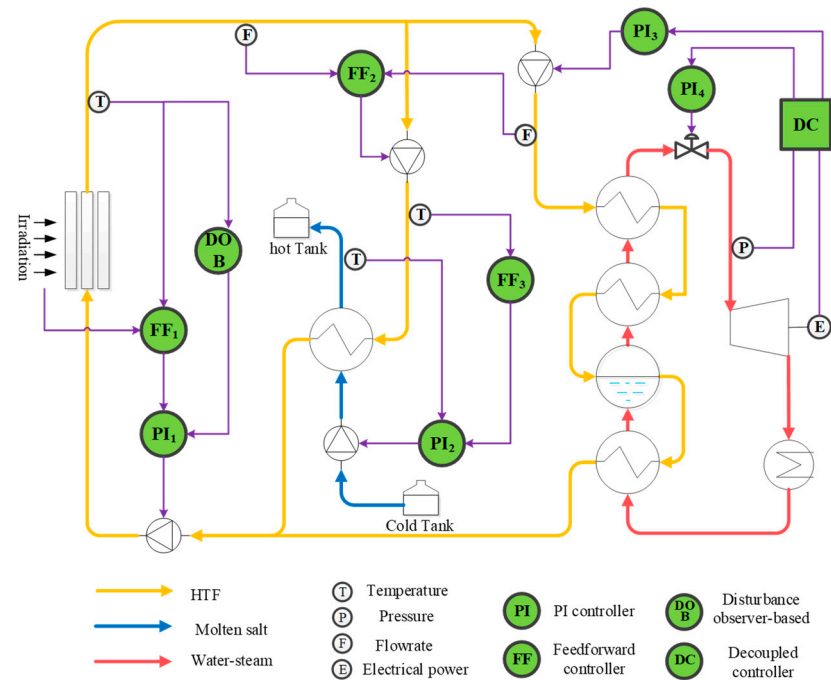
Figure 7. Schematic diagram of the coordinated control strategy for the CSP-TES system.

3.1. DOB-Based Feedforward–Feedback Control Scheme of SF

Disturbance rejection is a common issue that exists in almost all control practices. In general, disturbance is categorized into internal disturbance, such as model mismatch and parameter perturbation, and external disturbance. Measurable external disturbance can usually be compensated by a feedforward strategy. However, the unmeasurable external and internal disturbance are challenging to fully eliminate. The CSP-TES system is a solar-driven system, which means there is unavoidable large external disturbance. Moreover, large variation in solar irradiation causes off-design operation conditions, resulting in certain internal disturbance. The large external and internal disturbances together put great challenges on the control of the CSP system. To solve the problem, a disturbance observer-based feedback–feedforward control strategy is proposed for the SF of the CSP system, of which the block diagram is illustrated in Figure 8.
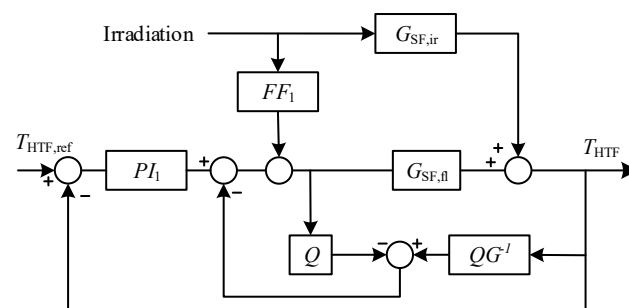
Figure 8. Block diagram of disturbance observer-based feedforward–feedback control scheme of the SF subsystem.

As can be seen, measurable solar radiation is compensated by the feedforward method to reduce its influence in time. However, the feedforward approach can only reject the measurable disturbance. In order to reduce the influence of unmeasurable disturbance, a disturbance observer is designed to obtain the equivalent disturbance. The disturbance estimated by the observer is then sent to the input as an additional control signal to compensate for the estimated disturbance. Finally, the outlet HTF temperature is fed back to the feedback controller to further boost the performance of disturbance attenuation.

Transfer functions $G_{SF,ir}$ and $G_{SF,fl}$ can be easily identified from the single-input single-output step response of the CSP-TES system under the open loop condition, accordingly. The issue is the design of the controllers FF_1 and PI_1, and the filter Q.

From the dynamic analysis, we found that $G_{SF,ir}$ and $G_{SF,fl}$ are relatively simple and can be identified as the first order process. In this way, the feedforward controller can be designed according to the invariance principle, namely

$$FF_1(s) = -\frac{G(s)_{SF,ir}}{G(s)_{SF,fl}} \tag{1}$$

where $G_{SF,ir}$ is the transfer function from irradiation to outlet HTF temperature, and $G_{SF,fl}$ is the transfer function from HTF flowrate to outlet HTF temperature of *SF*. G^{-1} is the inverse of $G_{SF,fl}$. FF_1 is the feedforward controller, PI_1 is the feedback controller, and Q is a filter.

Filter Q is the core of the disturbance observer and determines the robustness and anti-interference of control performance. To guarantee physical realizability, its relative order must not be lower than $G_{SF,fl}$. In this work, the filter is designed in the following form:

$$Q = \frac{1}{1 + \beta s} \tag{2}$$

where β is designed according to ref. [23].

Since the block diagram is established based on a linear system, the disturbance estimator and the feedback controller can be designed, respectively, according to the principle of superposition. Therefore, PI_1 is designed based on the identified transfer function $G_{SF,fl}$ and tuned manually. With this control scheme, the disturbance on the SF outlet HTF temperature can be attenuated rapidly.

3.2. Decoupling Control Scheme of PB

Flexible operation of the CSP-TES system directly depends on the flexible response of PB to grid commands. As PB has similar characteristics to conventional plants, the coordination idea is stimulated where the HTF flowrate majorly contributes to the electricity tracking, while the main valve largely controls the main steam pressure. To achieve the control purpose, a decoupling control scheme is proposed here, as demonstrated in Figure 9, where G is the transfer function matrix, D is the decoupling matrix, and PI_3 and PI_4 are the controllers.

Figure 9. Block diagram of decoupling control scheme of the PB subsystem.

Elements of the transfer function matrix can be identified from the step response of control variables, respectively, and also based on the open loop simulation of the simplified dynamic model in ref. [22]. Note that the inlet HTF temperature of PB is set as a constant during the identification simulation. In this way, the relationship between control and controlled variables is expressed as below:

$$\begin{bmatrix} E \\ P \end{bmatrix} = \begin{bmatrix} G_{11}(s) & G_{12}(s) \\ G_{21}(s) & G_{22}(s) \end{bmatrix} \begin{bmatrix} u_1 \\ u_2 \end{bmatrix} \tag{3}$$

where u_1 and u_2 are the HTF flowrate and opening of the main valve, respectively; and E and P are the electricity generation and steam pressure, respectively.

The non-diagonal elements indicate the coupling effect between the controlled variables. To eliminate the non-diagonal effect, a compensation method is applied. This approach treats the coupling effects as the feedforward signal, and compensates it by choosing a proper decoupling compensation matrix, as shown in the block diagram of the control structure given in Figure 9. Here, the coupling effect is fully eliminated by setting D_{11} and D_{22} as 1, and

$$D_{12}(s) = -\frac{G_{12}(s)}{G_{11}(s)}, D_{21}(s) = -\frac{G_{21}(s)}{G_{22}(s)} \tag{4}$$

Having deigned the decoupling matrix, the original coupled controlled issue is degraded to two independent single-input single-output problems, where the PI_3 and PI_4 can be designed conveniently.

3.3. Feedforward-Feedback Control Scheme of TES

From the CSP overall control strategy diagram, it can be seen that the HTF flowrate of the PB subsystem is responsible for power tracking, while the HTF flowrate of the SF is responsible for regulating SF outlet HTF temperature. The difference between the two flowrates are then delivered into the TES subsystem. Therefore, for the TES subsystem, the HTF flowrate is not controllable but depends on system operation conditions. Consequently, it is treated as a feedforward signal for the controller of TES. In order to ensure the efficiency of the TES subsystem, it must control the MS flowrate to compensate the influence of varying HTF flowrate. In addition, the measurable HTF temperature also serves as a feedforward signal to improve control performance of the TES subsystem. Finally, the block diagram of the feedback–feedforward control scheme of the TES subsystem is shown in Figure 10.

Figure 10. Feedback–feedforward control scheme of the TES subsystem.

According to the block diagram, disturbance of HTF flowrate and HTF temperature can be eliminated theoretically based on the invariance principle. By proper identification, the feedforward compensator can be designed as

$$FF_2 = -\frac{G_{TES,fl}(s)}{G_{TES,hx}(s)}, FF_3 = -\frac{G_{TES,tem}(s)}{G_{TES,hx}(s)} \tag{5}$$

where $G_{TES,hx}$ is the transfer function from MS inlet flowrate to MS outlet temperature, $G_{TES,fl}$ is the transfer function from HTF flowrate to HTF outlet temperature, and $G_{TES,tem}$ is the transfer function of SF outlet HTF temperature to MS outlet temperature. FF_2 and FF_3 are feedforward compensators for HTF temperature and flowrate, respectively. PI_2 is the feedback controller.

Similar to the feedback controller of SF, PI_2 is designed and tuned on the basis of $G_{TES,hx}$.

4. Simulation Results

In order to prove the rationality of the proposed control strategy, it was applied to the simplified dynamic model in ref. [22]. Apart from the steady-state operating parameters, as shown in Table 1, Table 2 gives the tuned parameters of the designed controllers. Simulation results of the CSP-TES system with a control period equal to 10 s are analyzed as follows.

Table 2. Parameters of the designed controllers.

Controller	Forms	Value
PI_1	$K_p + \frac{K_I}{s}$	$Kp = -24.243, K_I = -0.088$
PI_2	$K_p + \frac{K_I}{s}$	$Kp = -60, K_I = -0.78$
PI_3	$K_p + \frac{K_I}{s}$	$Kp = 0, K_I = 0.249$
PI_4	$K_p + \frac{K_I}{s}$	$Kp = 0.524, K_I = 0.011$
FF_1	$\frac{b_{10}+b_{11}s}{a_{10}+a_{11}s}$	$b_{10} = 1.394, b_{11} = 0.010;$ $a_{10} = 1.394, a_{11} = 0.006$
FF_2	$\frac{b_{20}+b_{21}s}{a_{20}+a_{21}s}$	$b_{20} = -19.70, b_{21} = -0.0592;$ $a_{20} = -16.943, a_{21} = -0.0625$
FF_3	$\frac{b_{30}+b_{31}s}{a_{30}+a_{31}s}$	$b_{30} = 61.50, b_{31} = 0.1112;$ $a_{30} = 1, a_{31} = 0.0105$
Q	$\frac{1}{1+\beta s}$	$\beta = 50$

4.1. Wide-Range Load Variation Tracking

The first case is used to illustrate that the coordinated control strategy proposed in this paper can realize flexible operation of the CSP-TES system under a wide range of load variation. As shown in Figure 11a, the electricity generation setting steps up from 41.8 MW to 42.8 MW at 1000 s. At 3000 s, the electricity generation and the main steam pressure increase from 42.8 MW to 50.8 MW at a rate of 0.4 MW/min, and from 9.4 MPa at a 0.045 MPa/min rate to 10.3 MPa, respectively, and then remain at 50.8 MW and 10.3 MPa accordingly. Meanwhile, the settings of MS outlet temperature and SF outlet temperature remain unchanged. Under such wide range load variation, simulation results of the manipulated variables and controlled variables are plotted in Figure 11. It can be seen that the actual electricity generation can track the step change with a slight overshoot, and the rise time is only about 150 s. The main steam pressure also has a good tracking performance with respect to step change. However, given a ramp change, the decoupling controller of the PB subsystem cannot realize the offset free control; the maximum deviations of the electricity and pressure during the ramp change are about 0.4 MW and 0.088 Mpa, respectively. Moreover, the overshoot of both after the ramp change are within 1%. More importantly, the maximum errors of the SF outlet temperature and the MS temperature are only within 0.5 °C, even under such a wide range of load variation, suggesting that the DOB works very well to reject disturbance.
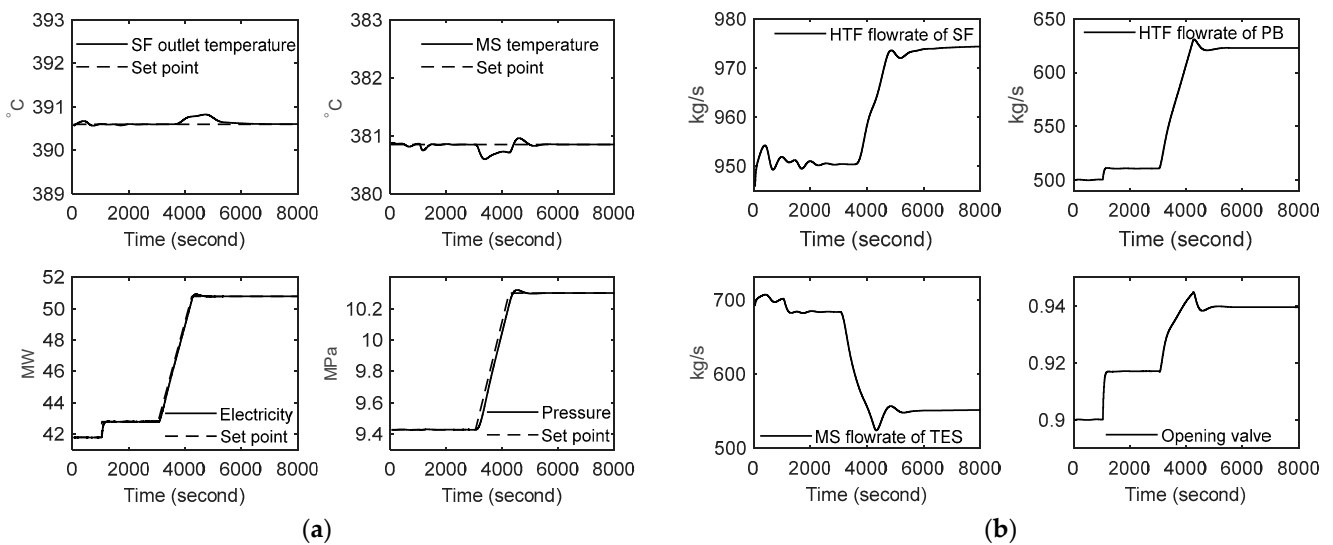
Figure 11. Simulation of wide-range load variation tracking: (**a**) the controlled variables; (**b**) the manipulated variables.

These performances are realized by proper adjustment of the manipulated variables, which is given in Figure 11b. As can be seen, HTF flowrate to PB is in line with the changing trend of electricity generation as more energy is needed for PB. Similarly, the trend of the opening valve agrees with that of the main steam pressure. For the MS outlet temperature, more HTF flowrate to PB leads to less flowrate to TES; consequently, the MS flowrate is regulated to maintain the MS outlet temperature. Varying operation conditions and the redistribution of HTF flowrate to PB and TES together cause various disturbance, especially the changes in SF inlet temperature. To reject these disturbances, the disturbance observer of SF estimates and compensates for them, causing changes in the total HTF flowrate and SF outlet HTF temperature. These manipulated variables are all in smooth variation, indicating the quality of the proposed control strategy.

4.2. Disturbance Rejection Performance

The biggest difference between CSP-TES systems and conventional plants is that energy input of CSP is uncontrollable and subject to strong uncertainty. Therefore, the proposed control strategy must meet the disturbance rejection performance, which is the purpose of the second case. Specifically, at 500 s, 2000 s and 3500 s, the step, ramp and sinusoidal changes of irradiation disturbance are simulated as illustrated in Figure 12. It can be seen that the electricity generation and main steam pressure can still maintain the setpoint tightly with a minor error for the step and ramp disturbance, as shown in Figure 13a. However, the sinusoidal disturbance cannot be rejected completely. Nevertheless, this disturbance can be suppressed greatly with the maximum error of about 0.4 MW and 0.06 MPa accordingly, even under the maximum amplitude increment of 50 W/m^2. In addition, the maximum deviation of both SF outlet temperature and MS temperature are about 1 °C, demonstrating that the control strategy has good disturbance rejection performance.

Due to the decentralized control structure, the task of disturbance rejection is mainly undertaken by SF and TES subsystems. As a measurable disturbance, the change in solar irradiation is fed forward to the SF inlet HTF flowrate rapidly. The feedforward compensation makes the trend of total HTF flowrate consistent with that of solar irradiation, as proven in Figure 13b. For the TES subsystem, as the electricity generation remains almost a constant, the uncontrollable surplus HTF flowrate is delivered to the TES subsystem, which explains why MS flowrate has a similar trend with total HTF flowrate. Despite disturbance observer and feedforward compensation, such strong external disturbance inevitably causes much more complicated lump disturbance, leaving SF outlet HTF temper-

ature and MS temperature fluctuating around the set-point. Nevertheless, all the control performances are satisfying in engineering practice. This demonstrates that the CSP-TES system can guarantee tracking performance under the proposed control strategy, even subject to strong disturbance.
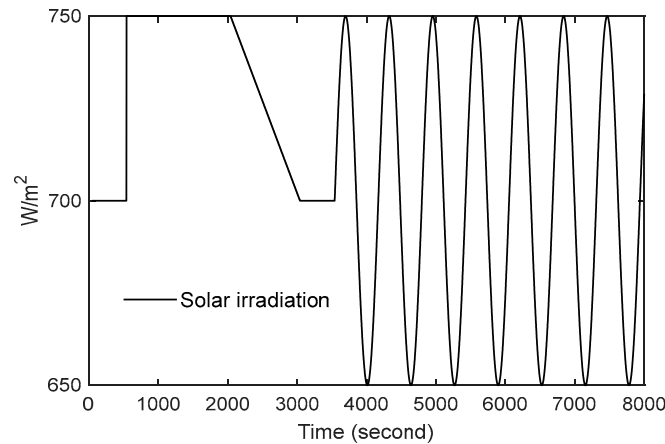
Figure 12. Profile of the step, ramp and sinusoidal disturbance of solar irradiation performance.
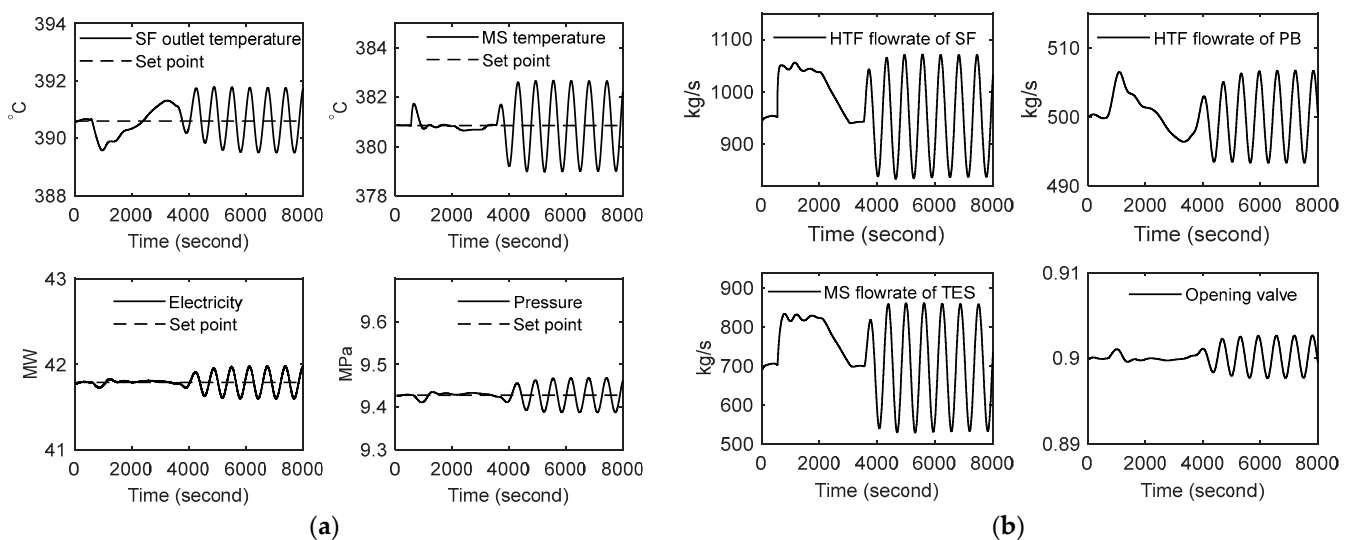
Figure 13. Simulation of disturbance rejection performance: (**a**) the controlled variables; (**b**) the manipulated variables.

4.3. Wide-Range Load Variation Subject to Disturbance

In order to simulate actual operating conditions, the third example studies the wide range load variation under the profile of the solar irradiation disturbance in Figure 14 and the setting profile of electricity generation and main steam pressure in Figure 15a. As already analyzed above, CSP-TES is a weak coupling system, and TES plays a critical role in decoupling SF and PB subsystems. With an elaborate control scheme of TES, the disturbance rejection performance is mainly confined by the SF subsystem, while the tracking task largely relies on the coordination control of the PB subsystem. Consequently, the overall system control performance will be similar to that of the two cases above, even when the set-point tracking and disturbance rejection tasks both exist. This is proven in the simulation results in Figure 15. As can be seen, the electricity generation and the pressure can track the set-points very well, although with minor perturbation around the set-points, which is similar to the first case. At the same time, the total HTF flowrate is adjusted frequently to compensate for solar irradiation change. However, as analyzed in

the second case, the influence of uncertainty and the large variation of solar energy mostly affects the SF outlet HTF temperature and MS temperature. Moreover, the magnitude of the fluctuation can be well attenuated, even under such strong disturbance, as the maximum error of the SF outlet HTF temperature and MS temperature are both within 3 °C, which is quite acceptable in engineering practice. There are also differences, as the fluctuation degree of the third case is more intense than that in the second case. Because the power tracking task causes a change of SF inlet HTF temperature, this means additional disturbances have to be estimated by the DOB compared with the second case, which burdens the disturbance observer. Nevertheless, the step and ramp changes of the electricity can be well tracked tightly and steadily, demonstrating the capacity of the proposed control strategy to achieve flexible operation of the CSP-TES system.
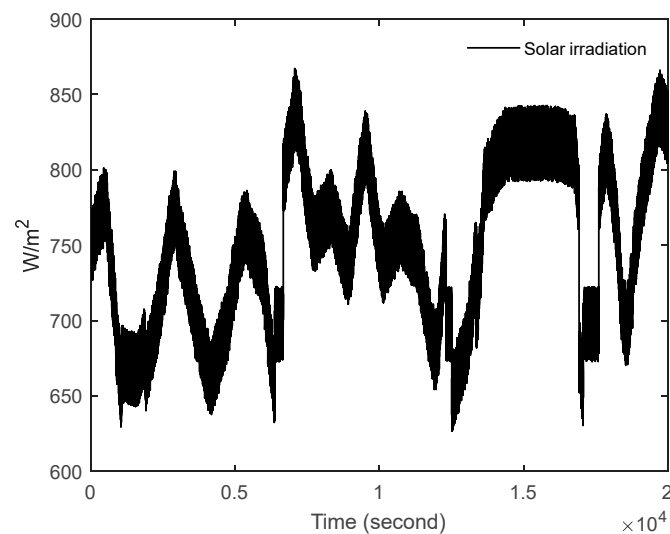
Figure 14. Profile of the simulated solar irradiation disturbance.

(**a**)

(**b**)
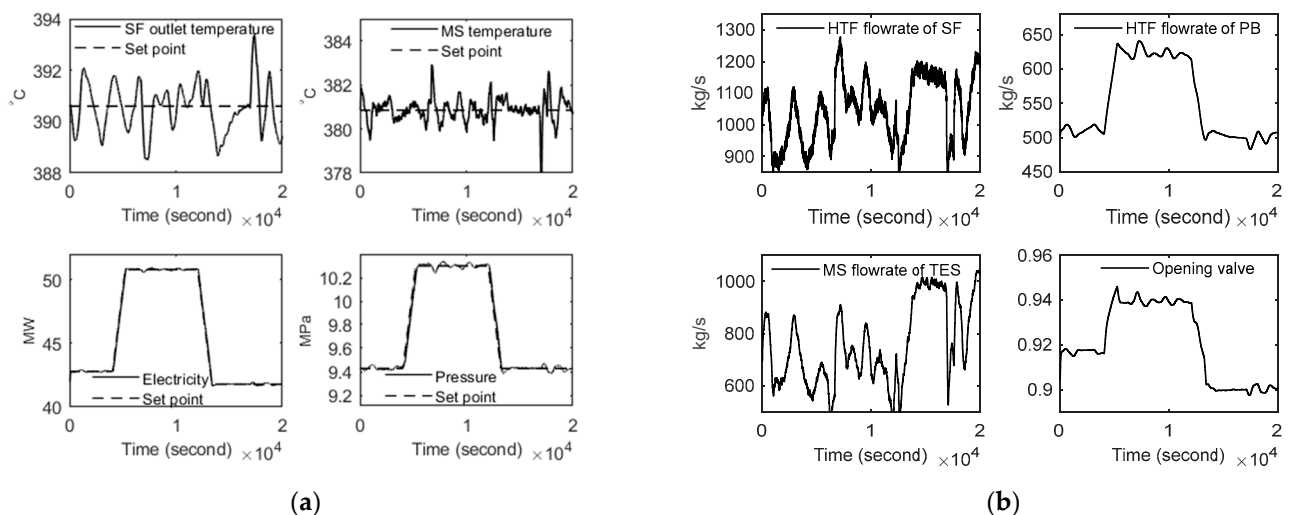
Figure 15. Simulation of wide-range load variation tracking subject to disturbance: (**a**) the controlled variables; (**b**) the manipulated variables.

5. Conclusions

Different from existing research of CSP-TES systems, investigating the potential of CSP-TES systems to flexibly operate in grid system regulation is the core purpose of this research. To achieve this goal, this work first analyzed the dynamic characteristics of a CSP-TES system; specifically, step response of the HTF flowrate, HTF temperature of PB, opening of main valve and solar irradiation were studied. The results show that CSP

and conventional plants both have a multiple variable control problem with large inertial time, but the control problem of the CSP-TES system is more complex because of strong uncertainties and switch nonlinearity, despite its weak coupling. This indicates that the control tasks are not only the well-known disturbance rejection, but also the coordination of different subsystems to the flexible operation of the CSP system.

Afterwards, a decentralized coordinated control strategy was designed to realize the flexible operation of the CSP system. Specifically, a DOB-based feedforward and feedback control strategy was designed for SF, a feedforward-feedback scheme for TES, and decoupling control for PB. These control schemes were then implemented on a system-level analytical dynamic system. The simulation results demonstrate that the proposed control strategy had good disturbance rejection performance, and could realize the flexible operation of the CSP-TES system even under wide-range load variation or strong disturbance, or both.

However, with the transition of conventional economic operation from independent to flexible participation in grid regulation, the role transfer of the CSP-TES system will face many challenges. For instance, how to design advanced control strategies to realize the deep variable working operation of CSP-TES; how to optimize the configuration and fully tape the flexible potential of energy storage devices; and how the semi-controllable CSP system collaborates with uncontrollable renewable energy sources, such as wind power and photovoltaics, remains uncertain. These all require further in-depth study in the future.

Institutional Review Board Statement: Not applicable.

Informed Consent Statement: Not applicable.

Data Availability Statement: Not applicable.

Conflicts of Interest: The authors declare no conflict of interest.

References

1. Achkari, O.; Fadar, A.E. Latest developments on TES and CSP technologies–Energy and environmental issues, applications and research trends. *Appl. Therm. Eng.* **2019**, *167*, 114806. [CrossRef]
2. National Oceanic and Atmospheric Administration, [EN.OL]. Available online: https://www.noaa.gov/news/carbon-dioxide-levels-breach-another-threshold-at-mauna-loa (accessed on 10 March 2022).
3. Wei, S.; Li, Y.; Gao, X.Y.; Lee, K.; Sun, L. Multi-stage Sensitivity Analysis of Distributed Energy Systems: A Variance-based Sobol Method. *J. Mod. Power Syst. Clean Energy* **2020**, *8*, 895–905. [CrossRef]
4. Wei, S.; Li, Y.; Sun, L.; Zhang, J.; Shen, J.; Li, Z. Stochastic model predictive control operation strategy of integrated energy system based on temperature flowrate scheduling model considering detailed thermal characteristics. *Int. J. Energy Res.* **2020**, *45*, 4081–4097. [CrossRef]
5. Dong, Y.; Jiang, X.; Liang, Z.; Yuan, J. Coal power flexibility, energy efficiency and pollutant emissions implications in China: A plant-level analysis based on case units. *Resour. Conserv. Recycl.* **2018**, *134*, 184–195. [CrossRef]
6. Shrimali, G. Making India's power system clean: Retirement of expensive coal plants. *Energy Policy* **2020**, *139*, 111305. [CrossRef]
7. Brand, B.; Boudghene Stambouli, A.; Zejli, D. The value of dispatchability of CSP plants in the electricity systems of Morocco and Algeria. *Energy Policy* **2012**, *47*, 321–331. [CrossRef]
8. Dinter, F.; Gonzalez, D.M. Operability, reliability and economic benefits of CSP with thermal energy storage: First year of operation of ANDASOL 3. *Energy Procedia* **2014**, *49*, 2472–2481. [CrossRef]
9. McPherson, M.; Mehos, M.; Denholm, P. Leveraging concentrating solar power plant dispatchability: A review of the impacts of global market structures and policy. *Energy Policy* **2020**, *139*, 111335. [CrossRef]
10. Jesus Vasallo, M.; Manuel Bravo, J. A MPC approach for optimal generation scheduling in CSP plants. *Appl. Energy* **2016**, *65*, 357–370. [CrossRef]
11. Madaeni, S.H.; Sioshansi, R.; Denholm, P. Estimating the Capacity Value of Concentrating Solar Power Plants with Thermal Energy Storage: A Case Study of the Southwestern United States. *IEEE Trans. Power Syst.* **2013**, *28*, 1205–1215. [CrossRef]

12. Kuravi, S.; Trahan, J.; Goswami, D.Y.; Rahman, M.M.; Stefanakos, E.K. Thermal energy storage technologies and systems for concentrating solar power plants. *Prog. Energy Combust.* **2013**, *39*, 285–319. [CrossRef]

13. Kost, C.; Flath, C.M.; Möst, D. Concentrating solar power plant investment and operation decisions under different price and support mechanisms. *Energy Policy* **2013**, *61*, 238–248. [CrossRef]

14. Dominguez, R.; Baringo, L.; Conejo, A.J. Optimal offering strategy for a concentrating solar power plant. *Appl. Energy* **2012**, *98*, 316–325. [CrossRef]

15. Bai, J.; Ding, T.; Wang, Z.; Chen, J. Day-Ahead Robust Economic Dispatch Considering Renewable Energy and Concentrated Solar Power Plants. *Energies* **2019**, *12*, 3832. [CrossRef]

16. Tascioni, R.; Arteconi, A.; Del Zotto, L.; Cioccolanti, L. Fuzzy Logic Energy Management Strategy of a Multiple Latent Heat Thermal Storage in a Small-Scale Concentrated Solar Power Plant. *Energies* **2020**, *13*, 2733. [CrossRef]

17. Nevado Reviriego, A.; Hernández-del-Olmo, F.; Álvarez-Barcia, L. Nonlinear Adaptive Control of Heat Transfer Fluid Temperature in a Parabolic Trough Solar Power Plant. *Energies* **2017**, *10*, 1155. [CrossRef]

18. Gao, X.-H.; Wei, S.; Su, Z.-G. Optimal model predictive rejection control for nonlinear parabolic trough collector with lumped disturbances. *Trans. Inst. Meas. Control* **2021**, *43*, 1903–1914. [CrossRef]

19. Leo, J.; Davelaar, F.; Besancon, G.; Voda, A. Modeling and control of a two-tank molten salt thermal storage for a concentrated solar plant. In Proceedings of the 2016 European Control Conference (ECC), Aalborg, Denmark, 29 June–1 July 2016.

20. Li, L.; Li, Y.; Yu, H.; He, Y.-L. A feedforward-feedback hybrid control strategy towards ordered utilization of concentrating solar energy. *Renew. Energy* **2020**, *154*, 305–315. [CrossRef]

21. Sánchez, A.J.; Gallego, A.J.; Escaño, J.M.; Camacho, E.F. Event-based MPC for defocusing and power production of a parabolic trough plant under power limitation. *Sol. Energy* **2018**, *174*, 570–581. [CrossRef]

22. Wei, S.S.; Liang, X.F.; Mohsin, T.; Wu, X.; Li, Y.G. A simplified dynamic model of integrated parabolic trough concentrating solar power plants: Modeling and validation. *Appl. Therm. Eng.* **2020**, *169*, 114982. [CrossRef]

23. Wu, X.; Shen, J.; Sun, S.; Li, Y.; Lee, K.Y. Data-Driven Disturbance Rejection Predictive Control for SCR Denitrification System. *Ind. Eng. Chem. Res.* **2016**, *55*, 5923–5930. [CrossRef]